Desalination and Water Treatment
www.deswater.com

doi: 10.5004/dwt.2023.29197

282 (2023) 70–79
January

Experimental study of a solar desalination unit based on humidification–dehumidification by underground condensation

Abdelmotaleb Ajengui[a,b,*], Rym Ben Radhia[a,b], Sirine Saidi[a,b], Belgacem Dhifaoui[a,b], Sadok Ben Jabrallah[a,b]

[a]*Laboratory of Energy and Heat-Mass Transfer, University of Tunis El Manar, 1060 Tunis, Tunisia, Tel.: 0021622665623; email: abdelmottaleb1@hotmail.fr (A. Ajengui), Tel.: 0021652528229; email: rymo2001@yahoo.fr (R.B. Radhia), Tel.: 0021652195907; email: sirine274@live.fr (S. Saidi), Tel.: 0021697753051; email: dhifaouib@gmail.com (B. Dhifaoui), Tel.: 0021698486708; email: sadok.benjabrallah@fsb.ucar.tn (S.B. Jabrallah)*
[b]*Faculty of Sciences of Bizerte, University of Carthage, 7021 Bizerte, Tunisia*

Received 15 March 2022; Accepted 21 November 2022

ABSTRACT

This work represents an experimental study of a desalination system based on humidification–dehumidification (HDH) using solar energy in the meteorological conditions of Bizerte, Tunisia. This system is essentially composed of a humidifier integrated into a solar collector (solar evaporator) and an underground condenser. The latter, in which moist air produced by the solar evaporator passed, was buried at a depth of 1.25 m. The vapor in the air was transformed into water while reaching the cold walls of the condenser pipe. Subsequently, water was collected at the ends of the pipe. The desalination system was equipped with a measurement system in order to conduct the experimental study. The thermal performance of the HDH desalination unit and the fresh water production were evaluated by measuring soil temperatures, liquid film in the evaporator, humidity and air velocity. Measurements were taken in forced convection. The evolutions of the liquid film temperature along the humidifier plate, the evaporated and the condensate mass flow rates were measured in this work. The influence of air velocity on the freshwater production by the desalination unit was also examined this study. It is shown that, at a velocity of 4.79 m/s, the maximum production capacity was equal to 9.38 kg/d and the maximum GOR of the desalination unit was 74%.

Keywords: Desalination; Forced convection; Solar energy; Underground condensation

1. Introduction

In recent years, the demand for fresh water has increased considerably due to the growth of the world population as well as the rapid urbanization and economic and industrial development. In fact, the annual total water available per capita has risen from 6,042 m^3, in 1947, to 1,545 m^3 in 2011. Thus, meeting the growing water demand of humans and environment has become one of the most important issues that governments and decision-makers should deal with [1] (e.g., Middle East, North Africa (MENA) region and particularly the Maghreb countries [2]).

Based on the statistical data, scientists assumed that, by 2025, two-thirds of the population will not have enough amount of fresh water [3]. Many countries will be unable to satisfy their citizens' demand for fresh water (e.g., India having almost 18% of the total world population and only 4% of the water resources) [4].

To solve this problem, the desalination of brackish water and seawater using desalination systems powered by solar

* Corresponding author.

energy can be a good alternative as, in the above-mentioned countries, solar energy resources are abundant and most of the inhabitants live mainly in coastal areas [5].

The desalination of seawater ensures sustainable fresh water production. In fact, every day, 23×10^6 m^3 are produced by reverse osmosis, multi-stage flash distillation and multi-effect distillation. Most of these technologies use fossil fuels in the desalination process, while only 0.02% utilizes renewable energies [6]. In addition, they are very expensive when employed to desalinate small amounts of fresh water. Thus, the humidification–dehumidification (HDH) desalination may satisfy low freshwater needs in decentralized demand areas.

It is a low-temperature process where the total required thermal energy can be obtained from solar energy. HDH was investigated by several numerical and experimental works. Systems used in this process differ in terms of the design of humidifiers and dehumidifiers, the nature and number of the employed solar collectors as well as in terms of their daily production.

For example, Yuan et al. [7] developed a mathematical model to examine the performance of a humidification–dehumidification solar desalination system. The latter is composed of two humidifiers, two condensers, a solar collector, a water tank and other components such as fans, pumps and cross valves. The profiles of the condensate flow rate as well as those of the daily and menstrual solar irradiation were determined in the conducted study. The obtained results showed that the production of drinking water increased by rising the flow rate of the cooling water and decreasing its temperature. The authors demonstrated also that the production of fresh water in the utilized system was of the order of 5.2 $L/m^2 \cdot d$, in June, and of the order of 2.7 $L/m^2 \cdot d$ in December.

Orfi et al. [8] investigated numerically and experimentally a solar desalination system based on humidification–dehumidification. This system contains two solar air and water collectors, a humidifier and a condenser. In the performed experiments, the temperatures and humidity at the inlet and outlet of the various components of the desalination system were measured and their change was depicted. A global mathematical model relying on the thermal and mass balances of air and water was also developed. The numerical results revealed that the optimal mass flow ratio corresponded to the maximum freshwater production.

Nafey et al. [9–21] studied numerically and experimentally an HDH solar desalination system installed in Egypt. The used experimental device is made up of a solar air collector, a solar water collector, a humidifier and a dehumidifier. The experiments were conducted to measure the temperature of the ambient air, the supply of water in the humidifier and that of the cooling water in the dehumidifier. The numerical study was based on the resolution of the energy and mass balances in the various components of the desalination unit. It demonstrated that the flow rate of the distillate increased with the augmentation of the flow rate of air and that of cooling water up to a maximum value equal to 0.05 kg/s. Beyond this value, the flow rate remained constant. The authors also developed a correlation to predict the unit productivity under different operating conditions. The production of this distiller was 7 kg/d.

Tahri et al. [10] studied numerically a condenser of an HDH solar desalination unit. The used condenser contains vertically-arranged 302 parallel pipes. The resolution of the energy and mass balances allowed testing the influence of the operating parameters on the system production. The authors revealed that the latter increased with the rise of the relative humidity and air flow rate and decreased with the increase in the temperature of the cooling water and water flow rate in the humidifier.

Zhani et al. [11–13] investigated numerically and experimentally an HDH solar desalination unit composed of two flat water and air solar collectors, an evaporator and a plate condenser. The aim of the research work was to monitor the functioning of the system during summer. The temporal evolution of air and water temperatures and the relative humidity at the inlet and outlet of each component of the employed system were also examined. The authors demonstrated that the maximum production of fresh water was 20.5 kg/d for surfaces of 16 and 12 m^2 of air and water solar collectors, respectively.

Saidi et al. [14–16] studied numerically and experimentally a solar desalination system based on humidification–dehumidification (HDH). This system consists of a humidifier integrated into a solar collector and a tubular dehumidifier. The experimental study allowed determining the profiles of water and temperature in the humidifier and in the dehumidifier and those of the evaporated water flows and condensate in natural and forced convection. The experimental study proved that the production of the desalination system increased with the air suction velocity. This production reached its maximum at 3.34 m/s. Then, it decreased to attain a value superior to 3.34. In order to carry out the numerical study, a mathematical model based on heat and mass balances was developed. The finite difference method was applied to discretize the equations and the resolution was carried out on the MATLAB software. The obtained results showed that the evaporated water and condensate flow rates in the desalination unit increased with the rise of air temperature and water supply in the humidifier. It was also observed that both flow rates first rose with the feed flow rate increase in the humidifier up to 5.5 kg/h. Then, they decreased beyond this value.

As the major problem of the HDH process consists in the condensation and, more precisely, in the choice of the appropriate type of condenser. The performance of condensation relying on a tubular condenser is low due to several parameters: temperature of the cooling water, exchange surface, corrosion of the pipes, thermal insulation of the walls and sealing. Therefore, it is necessary to develop another underground condensation system to solve the mentioned problems and, subsequently, to improve the condensation performance. This system was studied in several research works.

For instance, Lindblom et al. [17,18] examined experimentally and numerically a solar desalination system based on underground condensation. The desalinated water was employed for irrigation. It was obtained by evaporating seawater, while the humidified air was condensed in a system of underground pipes. In the numerical study, a global model of heat and mass transfer was used in the system

and MATLAB 6.5 software was utilized for the resolution. The study analysed the capacity of the IC system (condensation by irrigation) to produce drinking water. Numerical results showed that this system has an average water production capacity of 1.8 kg/d on a 50 m pipe.

The aim of the research work was to examine the influence of several parameters (e.g., the air temperature at the inlet of the condensing pipes, the solar radiation and the depth and spacing of the condensate pipes, etc.) on the production of the desalination unit. Experimental results revealed that the rise of air temperature at the inlet from 60°C to 72°C allowed obtaining a system production of 5.9 m/d that could be improved by increasing the depth and spacing of the condensate pipes.

Ocati et al. [19,20] studied numerically a solar desalination system based humidification–dehumidification. The system is composed of a solar humidifier and an underground condenser. The produced water was used for irrigation. The applied process consists, first, in vaporizing seawater in a solar humidifier. Then, the humid air condensed when passing through a set of underground pipes. Energy and mass balances were developed to describe the phenomena of evaporation and condensation in the desalination unit. The study was conducted to determine the profiles of the evaporated water and condensed flow rates as well as the temperature and humidity of the air entering the evaporator during the day.

Solar distillation is essentially based on two phenomena: evaporation and condensation. The improvement of these two phenomena allows enhancing the desalination system production. In a previous work [15] carried out in our laboratory, Saidi et al. [15] showed that when the system operates under the usual conditions, the condenser has a low energy performance, which limits the desalination unit production. The present work, presents a continuation of the previous study [15] in order to improving the efficiency of condensation. In this study, we propose to replace the tubular condenser used in Saidi et al. [15] by an underground condenser. We deal with underground condensation because it was not intensively examined in the literature and also to lower the condensation temperature and keep it stable all day long. In the present work, a solar desalination system based on humidification–dehumidification (HDH) by underground condensation was studied experimentally. The experimental device consists essentially of a humidifier integrated into a solar collector and an underground condenser (dehumidifier). The thermal performance and water production of the HDH unit are determined.

2. Experimental study

The studied system is a solar desalination unit based on humidification–dehumidification in the meteorological conditions of Bizerte, Tunisia (37.3° south latitude and 9.9° longitude). The unit comprises a solar evaporator and an underground coil-shaped condenser made of reinforced plastic. The evaporator was installed on a support forming an angle θ = 35° with the horizontal in order to capture the maximum amount of solar radiation. Then, the condenser was put underground, which allowed cooling its wall. The gas flow from the steam-laden humidifier condensed as it passed through the dehumidifier coil whose wall was cooler than the humid air.

2.1. Solar evaporator

The solar evaporator (presented in Fig. 1) has a parallel-piped shape with a length L = 2 m, a width l = 1 m and a height h = 0.22 m. It consists mainly of a flat sheet metal plate acting as absorber. A film of water flowed on the external wall of this plate thanks to a porous fabric that allowed the uniform wetting of the plate and avoided the formation of dry areas. A glass cover, acting as a solar collector, was exposed to the solar radiation. It was placed on a wooden frame that reduced the loss of steam. The sidewalls of the evaporator were made of two plates of MDF which is a pressed wood ensuring thermal insulation. In order to minimize heat loss, a layer of cork and a layer of wood were put on the backside of the absorber plate.

A fan allowed the circulation of a forced upward flow of air in the humidifier where it was in direct contact with the falling water film. The water supply in the evaporator was ensured by a constant-volume tank placed at a high position to make the water volume stable. This tank was linked to a horizontal copper pipe put on the absorber plate. The pipe was drilled by small-diameter holes allowing water to pass over the plate to form the liquid film to be evaporated. A valve was placed at the inlet of the evaporator to fix the feed water flow rate. To recover the brine, a plastic pipe was put below the evaporator, allowing its collection. The air was, then, humidified after the evaporation of the film exposed to solar radiation. Subsequently, the humidified air was directed towards the underground condenser.

2.2. Condenser

The desalination unit dehumidifier (Fig. 2) is an underground heat exchanger. The latter contains a condenser inclined in a well of a depth equal to 0.8 m, on one side, and 1.25 m on the other side. Its internal structure, having

Fig. 1. Image of the solar evaporator: 1-air inlet, 2-humid air outlet, 3-water supply, 4-glass, 5-brine recovery.

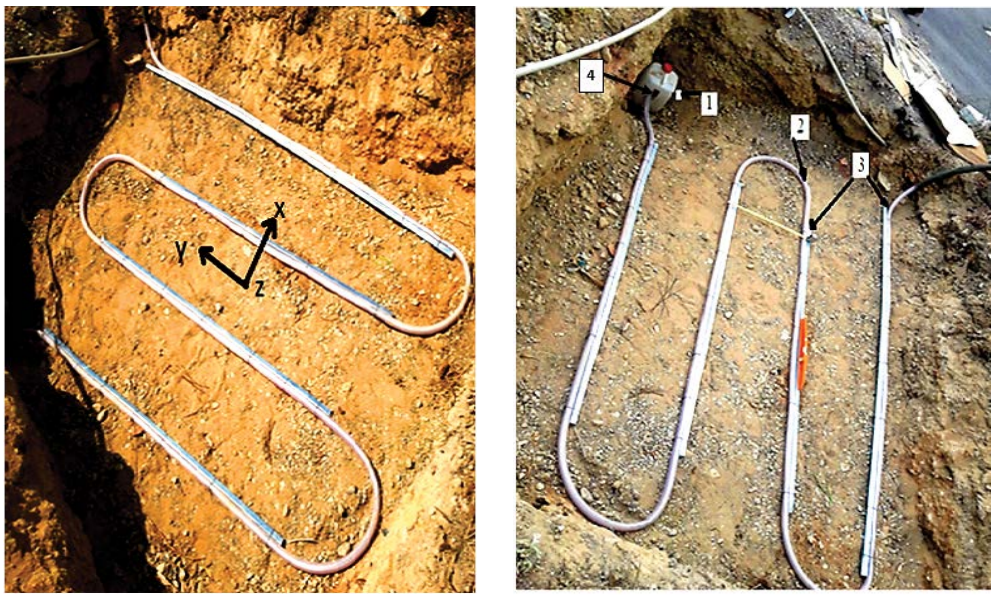

Fig. 2. Image of the underground condenser: 1-condensate collector, 2-pipe, 3-rods, 4-exit of dehumidified air.

the form of a coil, consists in a reinforced plastic pipe with an external diameter of 25 mm, a thickness of 2 mm and a length of 15 m. The inclination of the well bottom and coil facilitated the collection of the water droplets formed after condensation at the lower end of the pipe. Four aligned metal and inclined rods were used to fix the coil.

Moist air released from the solar evaporator circulated through the underground pipe that was in direct contact with the cool soil, which made it cool and condensed. The condensate was accumulated using a collector placed at the lower end of the pipe.

The inclination of the condenser coil pipe that recovered water droplets by easy circulation is presented in Fig. 3. It was ensured as follows:

Point A, having a depth of 0.8 m, was fixed on the high side of the well. Point B was inclined with respect to point A with a depth of 3.5 cm. Point C was inclined with respect to point B according to the inclination of the well. However, point D was inclined with respect to C, point F with respect to E and point H with respect to G. These points had the same inclination conditions as B with respect to A. Point E with respect to point D and point G with respect to point F have the same inclination as point C with respect to point B. Point H, having a depth of 1.25 m and used to guarantee the condensate recovery, was fixed on the low side of the well.

2.3. Measurement tools

To conduct the experimental study, the solar desalination unit was equipped with a measuring system comprising sensors of temperature, flow, humidity, solar radiation and air velocity. Ten K-type thermocouples (Chromel/Alumel) were put along the porous fabric covering the absorber plate to measure the liquid film temperature. Four other thermocouples were put inside the condenser. Two of them were used to measure the humid air temperature at the inlet and

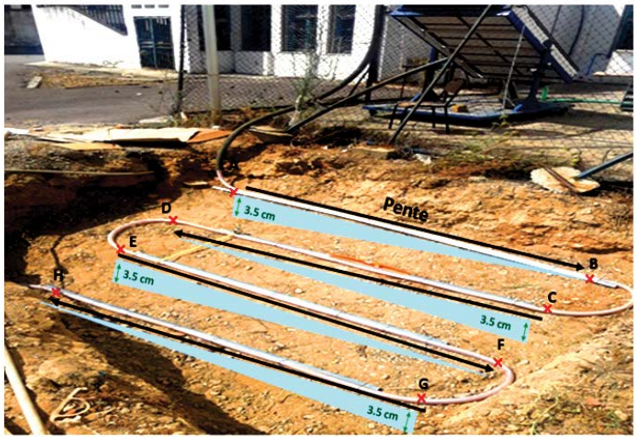

Fig. 3. Inclination of the condenser coil.

the outlet of the condenser. The other ones, with a 25 cm spacing, were utilized to measure the moist air temperature inside the condenser. Six thermocouples were installed to measure soil temperatures. All these thermocouples were connected to a data acquisition system that stored data every 20 min. Humidity and air velocity were measured by a TESTO445 digital multifunction device. An electronic scale and a stopwatch were employed to measure of feed water, brine and condensate the flow rates. To calculate the feed water flow rate in the humidifier, the water level was, first, set in the constant-level tank and, then, the flow control valve placed at the inlet of the humidifier was opened. Once the surface of the tissue was wetted, the water outlet was directed towards a beaker put on the electronic scale.

These flow measurements were taken early in the morning before sunlight reached the humidifier. The evaporated water flow rate was calculated by the difference between the flow rate of feed water and that of brine:

$$\dot{m}_e = \dot{m}_f - \dot{m}_b \quad (1)$$

where $\dot{m}_e$, $\dot{m}_f$ and $\dot{m}_b$ are the evaporated, feed water and brine mass flow rates.

Fig. 4 presents the image of the experimental device fitted with the measurement tools.

The characteristics and uncertainties of the measurement tools used in the experimental study are shown in Table 1.

Preliminary tests were performed to check:

- The adequate functioning of the feed water tank,
- Tightness of the device to water and vapor,
- The proper functioning of the measurement system,
- The reliability of the system by varying the operating parameters,
- The good wetting of the absorber plate.

3. Experimental results and discussions

3.1. Temperature variation

Fig. 5 shows the evolution of the earth surface temperature to a depth of 1.25 m. During 5 d of testing, the soil temperature decreases with depth and remains constant from (Z = 1 m). Due to the solar radiation that heated the ground surface, the highest temperature was recorded at (z = 0 m). It varied from 28°C to 25°C. Fig. 5 reveals that temperature decreases throughout the well and remains constant at a depth z = 1 m. Because of the earth inertia power, the temperature of the underground is more constant than that of the soil. It should be noted that the temperature at the bottom of the well remains the same (16°C). For this reason, the ground at the depth of 1 m can be used to cool the moist airflow coming from the evaporator and condense it. To ensure the results accuracy, the experiments were carried out on summer days during which the weather conditions were almost similar. The meteorological data (relative humidity H, ambient temperature T_{amb} and global solar irradiation G) obtained during the measurement days are shown in Table 2.

Fig. 4. Image of the used desalination unit and the measuring device: 1-evaporator, 2-pipe carrying humid air, 3-thermal insulation of the pipe, 4-underground condenser, 5-condensate recovery, 6-system acquisition of temperatures.

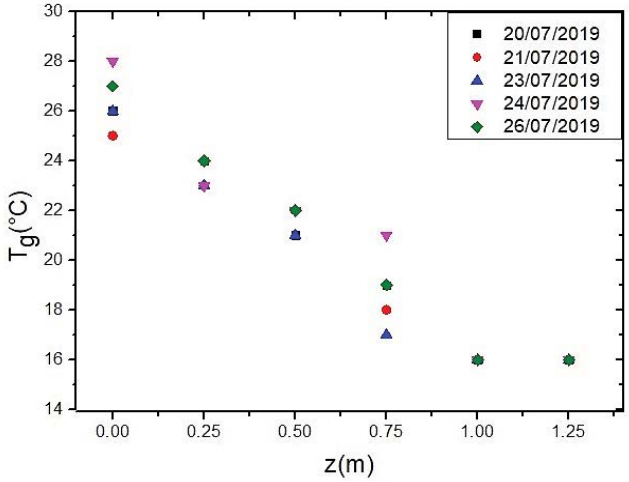

Fig. 5. Soil temperature evolution according to the depth during several days at 2 P.M.

Table 2
Meteorological data obtained on different measurement days having similar climatic conditions

Day	Relative humidity (%)	Ambient temperature (°C)	Global solar irradiation (kW/m²)
20/07/2019	44–59	25–36	0.52–0.93
21/07/2019	43–58	25–35	0.52–0.93
23/07/2019	46–61	24–35	0.55–0.93
24/07/2019	45–65	26–36	0.54–0.93
25/07/2019	48–62	26–34	0.54–0.93
26/07/2019	45–63	28–35	0.53–0.93
27/07/2019	46–68	27–35	0.49–0.93
28/07/2019	53–64	25–34	0.48–0.93

Table 1
Characteristics of the measuring tools

Instruments	Reference	Description	Accuracy
Thermocouple	Type K	Temperature	±0.5°C
Hygrometer	TESTO445 capacitance probe	Relative humidity	±2%
Air velocimeter	TESTO445 hot wire probe	Air velocity	±0.05 m/s
Digital balance	PB1501-T2202	Mass	±0.1 g

The results represented in Fig. 5 are confirmed by Fig. 6 representing the evolution of the soil temperature during 2 d at a depth of 1m and 1.25 m. Obviously, the two curves are merged and, on these 2 d, the temperature profile remains constant and equal to16°C.

Fig. 7 shows the variation of the liquid film temperature along the absorber plate of the humidifier for different air velocities V during several typical summer days at 1:00 P.M. The desalination unit operated in natural convection (V = 0 m/s) or forced convection (V = 1.8–9.2 m/s). During this study, several days having similar weather conditions were selected. The inlet of the falling liquid film corresponds to y = 0 m, while the airflow is counter current and enters the humidifier at y = 2 m. The temperature profile of the water film flowing along the humidifier remains the same at different air velocities even in case of natural convection. This figure also demonstrates that the falling liquid film can be divided into two zones. In the first one, called heating zone, the liquid temperature increases and the liquid film is heated without evaporation, which explains its temperature increase. This zone extends over the surface from the top of the evaporator to approximately y = 0.4 m which corresponds to the maximum liquid film temperature. The second zone is an evaporation zone where the temperature of the liquid film decreases due to its evaporation and the heat supplied by solar radiation is transformed into latent heat. These results were also obtained by [14,15,22–24].

Fig. 8 presents the liquid film temperature evolution T_f during the day at different positions y of the absorbing plate and the solar irradiation variation G in forced convection at air flow velocity equal to 2.7 8 m/s. The profiles of solar irradiation and that of the liquid film temperature are almost similar. In fact, the latter is characterized by the existence of two periods. In the first one, the temperature rises until around 1 P.M. On the other hand, the second period, which extends over the rest of the day, is marked by the decrease in the liquid film temperature due to the decrease of the solar radiation in the afternoon. It should be noted that the highest temperature profile was obtained at position y = 0.4 m where the maximum liquid film temperature falling along the humidifier was attained, as revealed in Fig. 7.

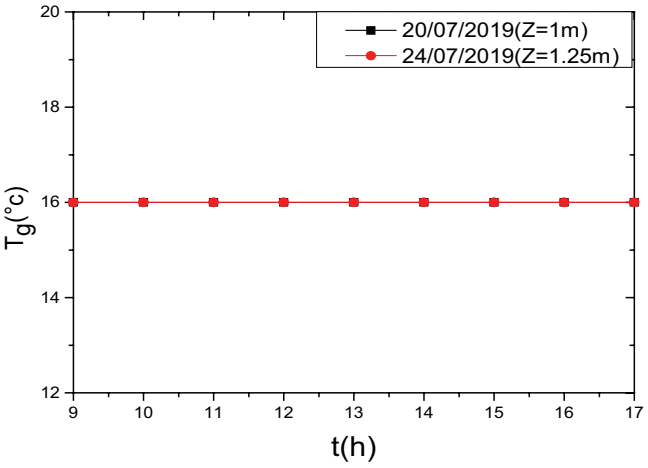

Fig. 6. Soil temperature profile during 2 d at a depth of 1 and 1.25 m, respectively.

3.2. Evolution of evaporated and condensate mass flow rates

Fig. 9 shows the variation of the evaporated mass flow rate and the global solar irradiation during 2 d characterized by almost similar climatic conditions and at two air suction velocities. The solar flux is the core of the evaporation phenomenon, hence the quantity of water evaporated on the liquid film streaming over the evaporation plate depends primarily on the solar flux absorbed. The obtained results demonstrate that the behaviour of the evaporated mass flow rate is similar to that of the solar irradiation with 1-h shift caused by the system thermal inertia. In the performed experiments, its maximum was reached at 2:00 p.m. as the maximum of solar irradiation was attained between 12:00 and 1:00 pm. It should be noted

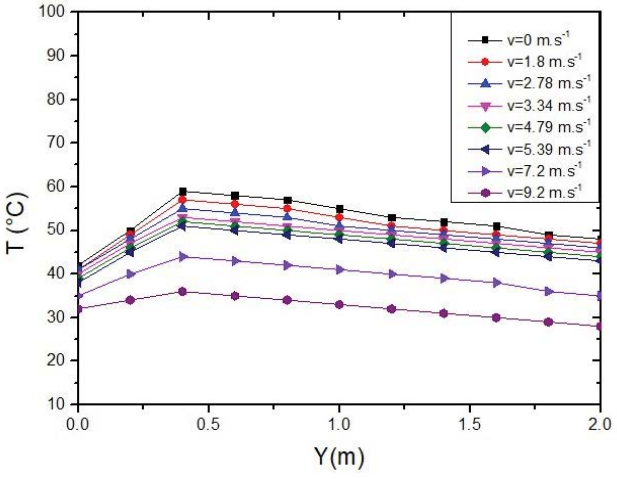

Fig. 7. The distribution of the liquid film temperature along the humidifier at 1 P.M. at different air velocities.

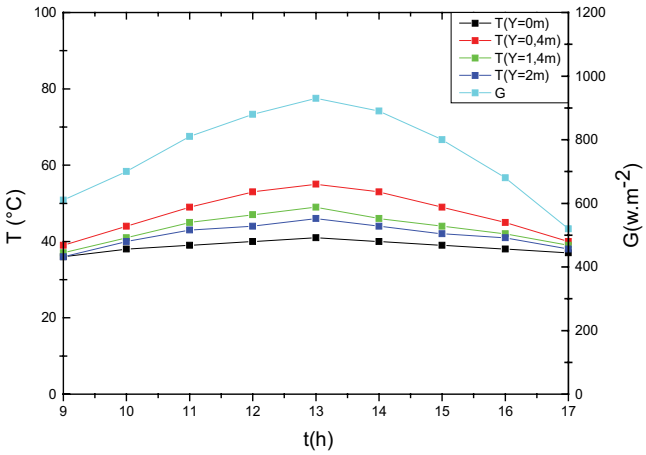

Fig. 8. Evolution of the liquid film temperature and the solar irradiation at V = 2.78 m/s during 21, July, 2019.

that the evaporated mass flow rate at a velocity of 3.34 m/s is lower than that obtained at a velocity equal to 4.79 m/s. Thus, forced convection improved the evaporation of the liquid film by about 10% between the two mentioned velocities. This result was confirmed by Saidi et al. [14,15] as well as by Wang et al. [25].

Fig. 10 depicts the evolution of the condensed mass flow rate $\dot{m}_c$ and the global solar irradiation during the day at an air flow velocity equal to 4.79 m/s. Since the condensate mass flow rate depends on the evaporated flow, its behaviour is the same as that of the evaporated mass flow rate of the water and solar radiation Indeed, its maximum was reached at 2:00 P.M., while that of global solar irradiation was attained at 1:00 p.m.

3.3. Air velocity effect on the cumulative fresh water production

To study the influence of air velocity on the cumulative fresh water production, experiments were carried out for several days in July 2019 characterized by similar climatic conditions.

Fig. 11 presents time evolution of the cumulative fresh water production at different air velocities. It shows that the cumulative freshwater production profile increases during the day until reaching its maximum equal to 9.38 kg at an inlet air velocity equal to 4.79 m/s. Beyond this value, the cumulative freshwater production is reduced. In fact, when the air velocity exceeds 4.79 m/s, the moist air contact time with the condenser pipe decreases and the water vapor does not have enough time to exchange heat. It is noted that, in case of natural convection, the production of the underground condenser is zero because of the pressure drop.

These results are confirmed by Fig. 12 where the cumulative freshwater production during the day is presented according to different air velocities.The maximum production of the desalination unit was obtained at 4.79 m/s.

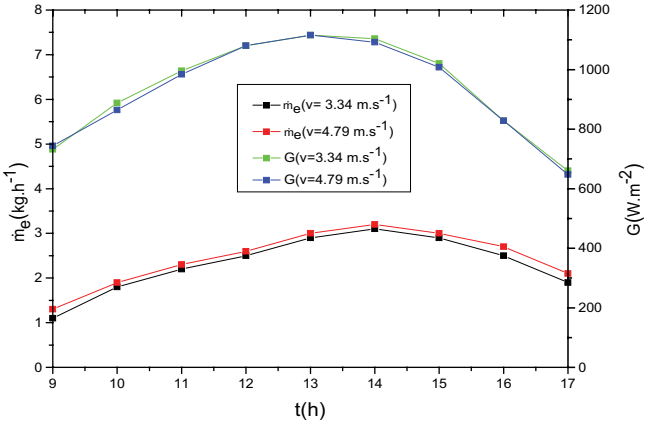

Fig. 9. Evolution of the evaporated mass flow rate and the global solar irradiation with respect to the day at two air velocities: (23, July, 2019, T_{amb} = 26°C–35°C, H = 46%–61%, $\dot{m}_f$ = 4.1 kg/h, V = 3.34 m/s) and (25, July, 2019, T_{amb} = 26°C–34°C, H = 48%–62%, $\dot{m}_f$ = 4.1 kg/h, V = 4.79 m/s).

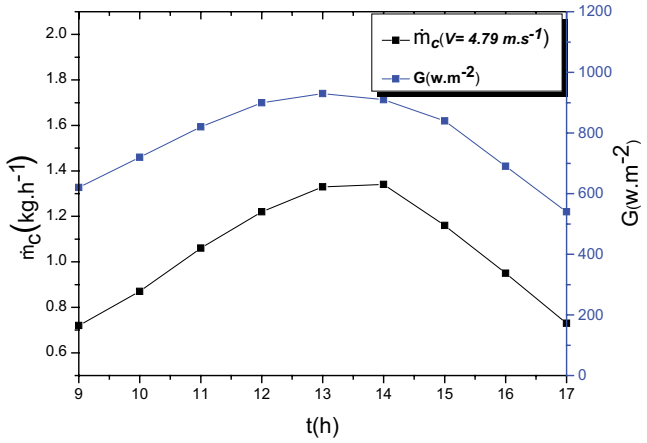

Fig. 10. Evolution of the condensed mass flow rate and the global solar irradiation during the day (25, July, 2019, T_{amb} = 26°C–34°C, H = 48%–62%, $\dot{m}_f$ = 4.1 kg/h, V = 4.79 m/s).

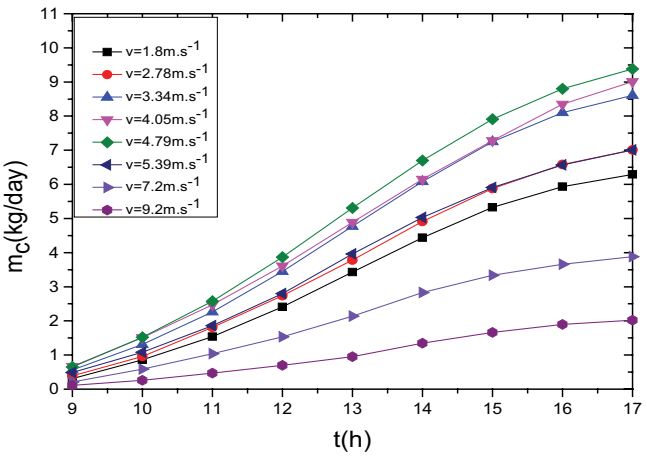

Fig. 11. Time evolution of the cumulative fresh water production at different air velocities (Table 2 presenting meteorological data).

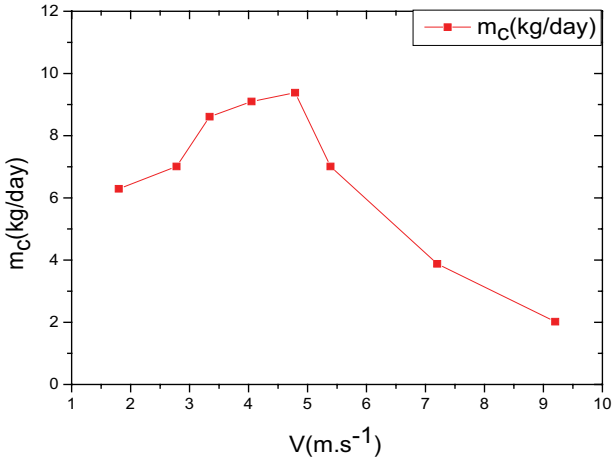

Fig. 12. Evolution of the fresh water daily production at different air velocities (Table 2 exposing the meteorological data).

3.4. Gained output ratio GOR

To estimate the desalination unit performance, the GOR, which is one of the most important parameters used to evaluate the thermal performance of desalination units, was calculated. In fact, GOR is the ratio of the latent heat of condensing the produced distilled water compared to the total heat absorbed by the humidifier [12]. This parameter is an index showing the amount of heat recovery in the desalination unit. The thermal performance of the desalination unit (GOR) is estimated in this study by the following formula [27]:

$$\mathrm{GOR} = \frac{\dot{m}_{\mathrm{ch_{fi}}}}{Q_i} \tag{2}$$

where h_{fi} is evaluated at the average temperature T of the condensate as shown [28]:

$$h_{\mathrm{fi}} = 2501.897149 - 2.40706403T + 1.092217\times10^{-3}T^2 - 1.5863\times10^{-5}T^3 \tag{3}$$

T in K and h_{fi} in kJ/kg.

Q_i, the flux absorbed by the water film, is given by the following equation:

$$Q_i = \alpha GS \tag{4}$$

where S is the evaporator area, G denotes the solar radiation and α is corresponds to the fictive absorptivity of the liquid film obtained by Khelif and Touati [29]:

$$\alpha = \tau_v\alpha_b + \tau_v\tau_b\alpha_p \tag{5}$$

where τ_v and τ_b are, respectively, the transmissivity of the glass and that of the brine, α_p and α_b are, respectively, the absorptivity of the absorbing plate and that of the brine with $\tau_v = 0.9$, $\tau_b = 0.68$, $\alpha_p = 0.95$ and $\alpha_b = 0.3$ [30].

Fig. 13 exposes the GOR temporal evolution during the three summer days, at V = 4.79, 3.34 and 1.8 m/s. The GOR values correspond to similar meteorological conditions during three days of July 2019. As the GOR is the ratio of the heat transferred by the condensation of the water vapor in the condenser divided by the total heat absorbed by the liquid water falling on the evaporator, it depends on the mass flow rate of the condensate and the solar flux. Since the latter is practically the same during the three days, the GOR has the same profile as the curve representing the condensate mass flow rate illustrated in Fig. 10. It is clear that the GOR increases during the morning until reaching its maximum. Then, it decreases for the rest of the day. It should be noted that the GOR exceeds the value of 86.87% when velocity is equal to 4.79 m/s at 1:00 p.m., while it is reduced at velocities equal to 3.34 and 1.8 m/s at 2:00 p.m. due to the increase in the above-mentioned condensation.

The GOR variation at different air velocities is illustrated in Fig. 14. Indeed, the best thermal performance is achieved at an optimum air velocity V = 4.79 m/s.

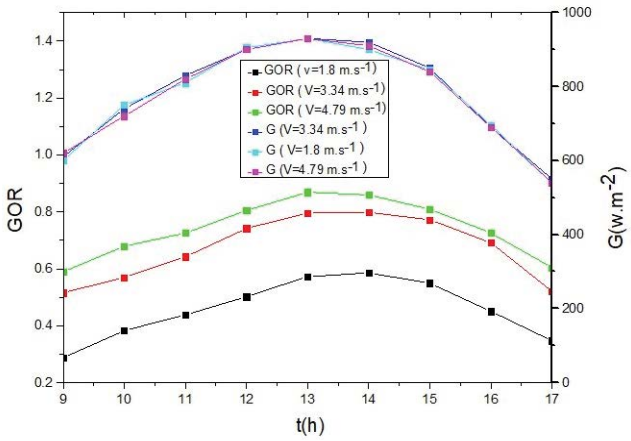

Fig. 13. Evolution of the gained output ratio (GOR) and the global solar irradiation during the day: (23, July, 2019 H = 46%–61%, $\dot{m}_f$ = 4.1 kg/h, V = 3.34 m/s); (20, July, 2019, H = 44%–59%, $\dot{m}_f$ = 4.1 kg/h, V = 1.8 m/s); (25, July, 2019 H = 48%–62%, $\dot{m}_f$ = 4.1 kg/h, V = 4.79 m/s).

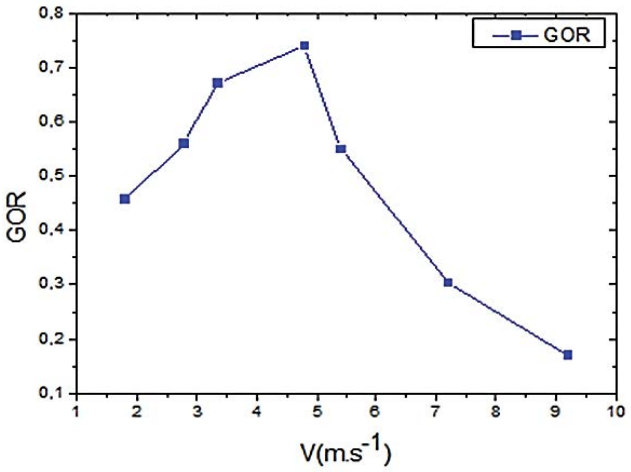

Fig. 14. Variation of the desalination system GOR according to air velocity.

The maximum value of GOR is 0.74, while that provided by Saidi et al. [15], using the same evaporator, is 0.65.

The GOR values presented in the literature are respectively 3 [11], and 4 or 2.6 with or without mass extraction by the study of Narayan et al. [31]. It is important to note that the studied desalination unit is an open water and air system without heating. However, the desalination unit investigated by Nayaran et al. [32] operated with the highest possible preheated brine temperature to ensure a maximum GOR of 4.

3.5. Comparison with literature

In the present study, the same evaporator designed in the work of Saidi et al. [15] is used. The authors mentioned that the energy performance of the evaporator was in the order of 80% while the condenser had a low energy performance that reduced the production of fresh water.

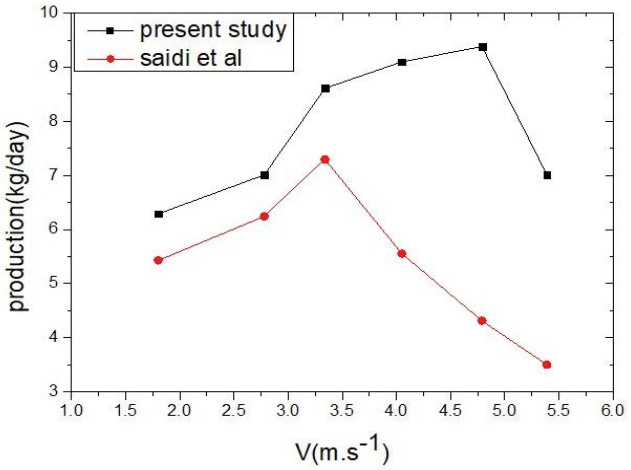

Fig. 15. Comparison of the results obtained in the present study and those provided by Saidi et al. [15].

For this reason, the aim of this study is to improve the condensation process by replacing the tubular condenser employed [15] by an underground condenser. To examine the performance of the underground condenser, the experimental results obtained in the present research work are compared to those provided by the study of Saidi et al. [15]. The daily productions of the desalination unit with respect to air velocity presented in the two works are compared in Fig. 15. The two profiles exhibit the same behavior since they increase to attain their maximum value. Then, they start decreasing. The daily production of the unit used in the present study is greater than that of the unit investigated [15]. In fact, it was improved by 4.27 kg at $V = 4.79$ m/s due to the fixing of the underground condenser wall temperature and the increase in the exchange wall between the moist air and the condensing surface. Indeed, in the present study, the underground condenser has a larger surface than that of the tubular condenser used [15].

The production of this unit is acceptable compared to that of small scale HDH desalination units. For example, the maximum production obtained by Saidi et al. [15] for the same humidifier is 7.29 kg/d, and that provided by Nafey et al. [21] under comparable climatic conditions is close to 8 kg/d, while that given by Nawayseh et al. [26] is 7.5 kg/d. In the present study, the use of the underground condenser in the humidification–dehumidification system allows enhancing the unit production.

4. Conclusion

In this research work, an experimental study of a small-scale humidification–dehumidification solar desalination system was performed. The unit using a measurement protocol was tested on the real site of Bizerte (Tunisia) during several days in summer characterized by almost similar climatic conditions. The experimental results showed the existence of a heating zone and an evaporating zone along the evaporator plate that supported the water film in the humidifier at different air velocities. The profiles of the evaporated and the condensed flows were determined and the influence of airflow velocity was highlighted. The optimum value of the air velocity at which the unit produced the maximum amount of fresh water was determined. This value equal to 4.79 m/s allowed obtaining a production of fresh water equal to 9.38 kg/d. The thermal performance of the desalination unit was studied in terms of GOR which an index showing the amount of heat recovery in the desalination unit. The maximum desalination unit GOR was equal to 74% at a velocity equal to 4.79 m/s. Finally, we may deduce that the change of the tubular condenser of the desalination unit to an underground condenser improved the daily production.

References

[1] A. Kettab, Les ressources en eau en Algérie: stratégies, enjeux et vision, Desalination, 136 (2001) 25–33.
[2] A.A. Abufayed, M.K.A. Elghuel, M. Rashed, Desalination: a viable supplemental source of water for the arid states of North Africa, Desalination, 152 (2003) 75–81.
[3] A. Pugsley, A. Zacharopoulos, J. Deb Mondol, M. Smyth, Global applicability of solar desalination, Renewable Energy, 88 (2016) 200–219.
[4] E.E. Delyannis, V. Belessiotis, Solar application in desalination: the Greek Islands experiment, Desalination, 100 (1995) 27–34.
[5] N. Ghaffour, V.K. Reddy, M. Abu-Arabi, Technology development and application of solar energy in desalination: MEDRC contribution, Renewable Sustainable Energy Rev., 15 (2011) 4410–4415.
[6] L. Garcia-Rodriguez, Seawater desalination driven by renewable energies: a review, Desalination, 143 (2002) 103–113.
[7] G. Yuan, H. Zhang, Mathematical modeling of a closed circulation solar desalination unit with humidification–dehumidification, Desalination, 205 (2007) 156–162.
[8] J. Orfi, M. Laplante, H. Marmouch, N. Galanis, B. Benhamou, S. Ben Nasrallah, C.T. Nguyen, Experimental and theoretical study of a humidification dehumidification water desalination system using solar energy, Desalination, 168 (2004) 151–159.
[9] A.S. Nafey, H.E.S. Fath, S.O. El-Helaby, A.M. Soliman, Solar desalination using humidification dehumidification processes. Part I. A numerical investigation, Energy Convers. Manage., 45 (2004) 1243–1261.
[10] T. Tahri, M. Douani, M. Amoura, A. Bettahar, Study of influence of operational parameters on the mass condensate flux in the condenser of seawater greenhouse at Muscat, Oman, Desal. Water Treat, 57 (2016) 13930–13937.
[11] K. Zhani, H. Ben Bacha, Experimental investigation of a new solar desalination prototype using the humidification dehumidification principle, Renewable Energy, 35 (2010) 2610–2617.
[12] K. Zhani, Solar desalination based on multiple effect humidification process: thermal performance and experimental validation, Renewable Sustainable Energy Rev., 24 (2013) 406–417.
[13] K. Zhani, H. Ben Bacha, T. Damak, Modeling and experimental validation of a humidification–dehumidification desalination unit solar part, Energy, 36 (2011) 3159–3169.
[14] S. Saidi, R. Ben Radhia, B. Dhifaoui, S. Ben Jabrallah, Experimental study of the inclined solar film evaporator, Desal. Water Treat, 56 (2014) 2576–2583.
[15] S. Saidi, R. Ben Radhia, B. Benhamou, N. Nafiri, S. Ben Jabrallah, Experimental investigation of a solar powered humidification–dehumidification desalination unit, Desal. Water Treat., 62 (2017) 1–10.
[16] S. Saidi, R. Ben Radhia, B. Benhamou, N. Nafiri, S. Ben Jabrallah, Numerical study of a solar desalination system by humidification–dehumidification, MATEC Web Conf., 330 (2020) 01045.
[17] J. Lindblom, B. Nordell, Water production by underground condensation of humid air, Desalination, 189 (2006) 248–260.

[18] J. Lindblom, B. Nordell, Underground condensation of humid air for drinking water production and subsurface irrigation, Desalination, 203 (2007) 417–434.
[19] V. Okati, S. Farsadd, Analysis of a solar desalinator (humidification–dehumidification cycle) including a compound system consisting of a solar humidifier and subsurface condenser using DoE, Desalination, 397 (2016) 9–21.
[20] V. Okati, S. Farsad, Numerical analysis of an integrated desalination unit using humidification dehumidification and subsurface condensation processes, Desalination, 433 (2017) 172–185.
[21] A.S. Nafey, H.E.S. Fath, S.O. El-Helaby, A.M. Soliman, Solar desalination using humidification–dehumidification processes. Part II. An experimental investigation, Energy Convers. Manage., 45 (2004) 1263–1277.
[22] S. Ben Jabrallah, A. Belghith, J.P. Corriou, Etude des transferts couple´s de matie`re et de chaleur dans une cavite´ rectangulaire: application a` une cellule de distillation (Study of coupled heat and mass transfer in a rectangular cavity: application to a distillation cell), Int. J. Heat Mass Transfer, 45 (2002) 891–904.
[23] A.S. Cherif, M.A. Kassim, B. Benhamou, S. Harmand, J.P. Corriou, S. Ben Jabrallah, Experimental and numerical study of mixed convection heat and mass transfer in a vertical channel with film evaporation, Int. J. Therm. Sci., 50 (2011) 942–953.
[24] R. Ben Radhia, J.P. Corriou, S. Harmand, S. Ben Jabrallah, Numerical study of evaporation in a vertical annulus heated at the inner wall, Int. J. Therm. Sci., 50 (2011) 1996–2005.
[25] J.H. Wang, N. Gao, Y. Deng, Y. Li, Solar power-driven humidification–dehumidification (HDH) process for desalination of brackish water, Desalination, 305 (2012) 17–23.
[26] N.K. Nawayseh, M.M. Farld, A.A. Omar, S.M. Al-Hallaj, A.R. Tamimi, A simulation study to improve the performance of a solar humidification–dehumidification desalination unit constructed in Jordan, Desalination, 109 (1997) 277–284.
[27] J. Koschikowski, M. Wieghaus, M. Rommel, Solar thermal-driven desalination plants based on membrane distillation, Desalination, 156 (2003) 295–304.
[28] G. Al-Enezi, H. Ettouney, N. Fawzy, Low temperature humidification dehumidification desalination process, Energy Convers. Manage., 47, (2006), 470–484.
[29] C. Khelif, B. Touati, Characterization of a greenhouse distiller, Rev. Renewable Energy, 1 (1998) 99–108.
[30] M. Zerrouki, N. Settou, Y. Marif, M.M. Belhadj, Simulation study of a capillary film solar still coupled with a conventional solar still in south Algeria, Energy Convers. Manage., 85 (2014) 112–119.
[31] G.P. Narayan, M.G.S. John, S.M. Zubair, J.H. Lienhard, Thermal design of the humidification dehumidification desalination system: an experimental investigation, Int. J. Heat Mass Transfer, 58 (2013) 740–748.
[32] G.P. Narayan, M.H. Sharqawy, E.K. Summers, J.H. Lienhard, S.M. Zubair, M.A. Antar, The potential of solar-driven humidification–dehumidification desalination for small-scale decentralized water production, Renewable Sustainable Energy Rev., 14 (2010) 1187–1201.